A New Three-Phase Interleaved Isolated Boost Converter With Solar Cell Application

K. Srinadh

***Abstract*— In this paper, a new three-phase high power dc/dc converter with an active clamp is proposed. The converter is capable of increased power transfer due to its three-phase power configuration, and it reduces the rms current per phase, thus reducing conduction losses. Further, interleaved operation of three-phase boost converter reduces overall ripple current, which is imposed into fuel cells and realizes smaller sized filter components, increasing effective operating frequency and leading to higher power density. Each output current of three-phase boost converter is combined by the three-phase transformer and flows in the continuous conduction mode by the proposed three-phase PWM strategy. An efficiency of above 96% is mainly achieved by reducing conduction losses and switching losses are reduced by the action of active clamp branches, as well. The proposed converter and three-phase PWM strategy are analyzed, simulated and implemented in hardware. Experimental results are obtained on a 500W prototype unit, with all of the design verified and analyzed.**

***Keywords*— three-phase dc/dc converter, isolated boost converter, interleaved operation, continuous conduction mode, three-phase PWM strategy**

I. INTRODUCTION

Fuel cells are identified as a future energy source due to their efficient and clean energy characteristics; furthermore, they produce low varying dc voltage in the range of 26 ~ 42 V for residential power application. Power conditioning system in the residential use usually consists of a low-voltage fuel cell as the primary source, a dc/dc converter to obtain isolated high voltage, and a dc/ac inverter to connect commercial ac voltage [1]. Since a dc/ac inverter supplies power into a 220V ac utility, an isolated dc/dc converter has to convert low varying dc voltage to high constant dc voltage at around 370 V. Therefore, a high power dc/dc converter with a high voltage ratio is needed, and a transformer is usually employed for boosting voltage as well as for isolation. Research has been focused on the three-phase dc/dc converter due to the benefits it can offer, such as high power density and high quality waveforms. However, most of the work thus far has been done on topology and PWM strategy for a voltage-fed dc/dc converter [2]-[5]. In recent, a three-phase current-fed dc/dc converter has been studied but it operates in the discontinuous conduction mode in spite of several advantages [6].

In this paper, development of a three-phase interleaved isolated boost converter with active clamp is proposed. Major features of the proposed converter include: (1) an increased power rating through employing a three-phase power transfer into dc/dc conversion, (2) a reduction of the ripple currents into the solar cells by an interleaved operation, (3) a reduction in conduction losses by continuous current conduction in the switches, transformer windings and input inductors, (4) an alleviated voltage surges and switching noises by three-phase active clamp branch, and (5) a lowering of the transformer turns-ratio by using voltage boost property inherited by boost topology. Due to these advantages, this converter is highly suitable for the interface between a low-voltage high-power solar cell source and an inverter load. It may also be extended to other low-voltage sources, such as batteries and photovoltaic which need high-voltage high-power dc/dc conversion capability.

II. PROPOSED 3-PHASE DC/DC CONVERTER

Fig. 1 shows the proposed three-phase interleaved isolated boost converter with active clamp. It consists of a three-phase dc/dc converter, whose outputs are connected to a three-phase full-bridge diode rectifier through a delta-delta wound three-phase transformer. The three-phase dc/dc converter is divided into a three-phase boost converter configured as three main MOSFET switches ($S_1 \sim S_3$) for three-phase boost converter, three auxiliary MOSFET clamp switches ($S_{C1} \sim S_{C3}$) and common clamp capacitor C_C for three-phase active clamp branch, and three dc boost inductors ($L_1 \sim L_3$) acting as a current source for each phase. Interleaved PWM operation occurs through the three dc boost inductors $L_1 \sim L_3$ of the three-phase boost converter and increases effective switching frequency of output current I_i of solar cells. Thus, it reduces overall ripple current, which is imposed into soalr cells and realizes smaller sized filter components. The active clamp branch reduces switching losses by zero voltage switching (ZVS) through the use of resonance between leakage inductances of the three-phase transformer and entire capacitances of clamp capacitance, output capacitances of MOSFET switches, and stray capacitances of the transformer. Furthermore, it clamps voltage across the switches and thus, no ancillary snubber is required in either the primary or secondary sides. The employed three-phase power structure increases input current and output voltage chopping frequencies by a factor of three and thus, reduces size of reactive filter

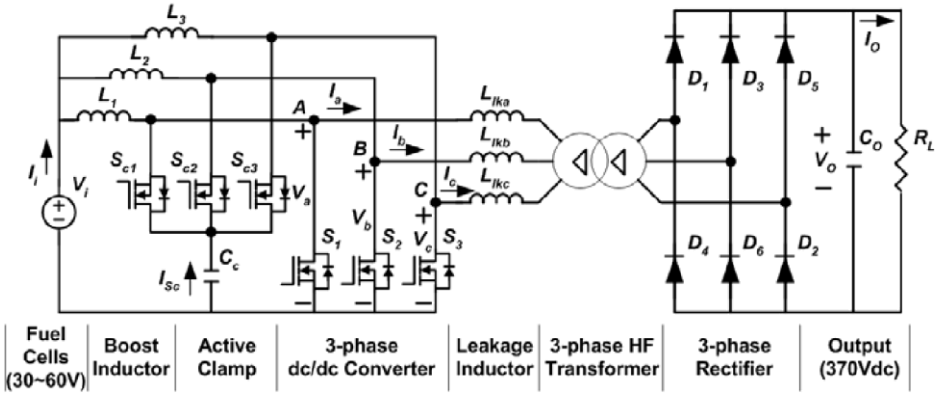

Figure 1. Power circuit configuration of three-phase isolated boost converter with active clamp

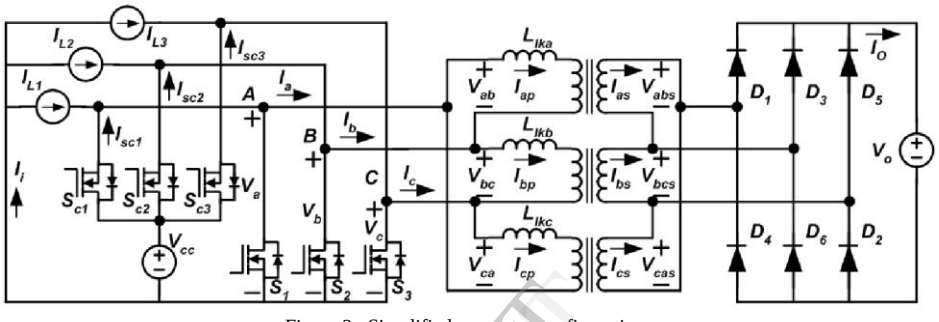

Figure 2. Simplified converter configuration

components; lowers rms current through the main switches and transformer windings by distributing currents into three-phase paths; increase power transfer capability with the same current rate and voltage rate of switch. In addition, continuous current conduction in three-phase converter output current $I_a \sim I_c$ and input current I_i leads to a highly efficient operation.

Due to these characteristics, the proposed converter is highly recommended as the interface between a low-voltage high-power solar cell source and a cascaded inverter stage. It is also suitable for other low-voltage sources, such as batteries and photovoltaic, which supply high-voltage, high-power dc to the next power stages.

III. PROPOPSED PWM STRATEGY

Fig. 2 shows a simplified circuit of the proposed three-phase isolated boost converter introduced in Fig. 1 and clamp capacitor C_C and output capacitor C_O are replaced by voltage sources V_C and V_O, respectively. The boost inductors $L_1 \sim L_3$ are also replaced by current sources $I_{L1} \sim I_{L3}$ respectively, during each switching period. Fig. 2 includes delta-delta connected three-phase transformer configuration, where i_{ap} represents the primary winding current in phase A and i_a is output current of boost converter in phase A.

Fig. 3 shows the ideal current waveforms of phase currents $i_a \sim i_c$ and transformer primary currents $i_{ap} \sim i_{cp}$; the gating signals $v_{G1} \sim v_{G3}$ for main switches $S_1 \sim S_3$, resulted phase voltages $v_a \sim v_b$ and line-to-line voltages $v_{ab} \sim v_{ca}$.

The operation procedure for the proposed converter is divided into 8 modes. Fig. 4 shows a set of eight topological states in phase A which occur during one switching interval T_S and analysis is focused on i_{ap}, the

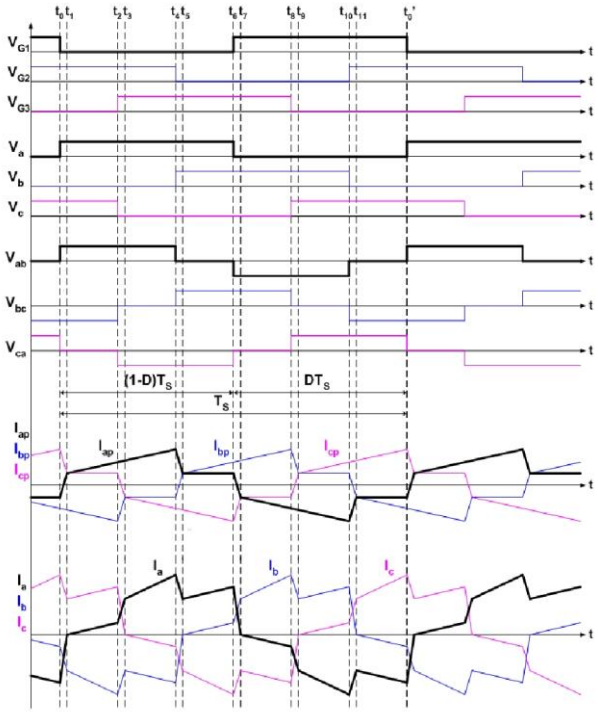

Figure 3. Ideal waveforms of the proposed converters

primary current of the transformer in phase *A*. The current paths of input boost inductors which are regarded as constant current sources are not marked to avoid complexity.

Before t_0 (Fig. 4 (h)) : The phase *A* main switch S_1 and phase *B* main switch S_2 are turned on. Thus, the boost inductor L_1 and L_2 charge energy from solar cells V_i. The transformer primary current of phase *A*, i_{ap} have been freewheeling through D_4 and D_6 because the line-to-line voltages of the phase, v_{ab} and v_{abs} are zero. The current i_{ap} have been flowing to the negative direction and has a constant value. The current of phase *C*, i_{cp} have been increasing.

$t_0 \sim t_1$ (Fig. 4 (a)) : At t_0, the phase *A* main switch S_1 turns off. The transformer primary line-to-line voltage v_{ab} reaches the positive value of clamp capacitor voltage V_{Cc} and v_{ca} becomes zero. On the other hand, the transformer secondary voltages v_{abs} and v_{cas} are being sustained at zero and $+V_o$ respectively. Thus, voltages across the leakage inductors L_{lka} and L_{lkc} are $+V_{Cc}$ and $-V_O'$ (reflected output voltage to the transformer primary) respectively. Due to the leakage inductance L_{lk}, finite time interval (T_1) is required and such a transition is called the current commutation time, which is $t_0 \sim t_1$. Equation (1) and (2) show the voltage magnitude of clamp voltage V_{Cc} and the current commutation time T_1 respectively. The transformer primary current, i_{ap} through the leakage inductance L_{lka} increases as a slope determined by the clamp voltage V_{Cc} as shown in (3). Equation (5) evaluates the current i_{ap} at t_1.

$$V_{Cc} = \frac{V_i}{1 - D} \quad (1)$$

$$V_O' = \frac{V_O}{n} \quad (2)$$

$$i_{ap} = \frac{V_{Cc}}{L_{lk}} t + i_{ap}(t_0) \quad (3)$$

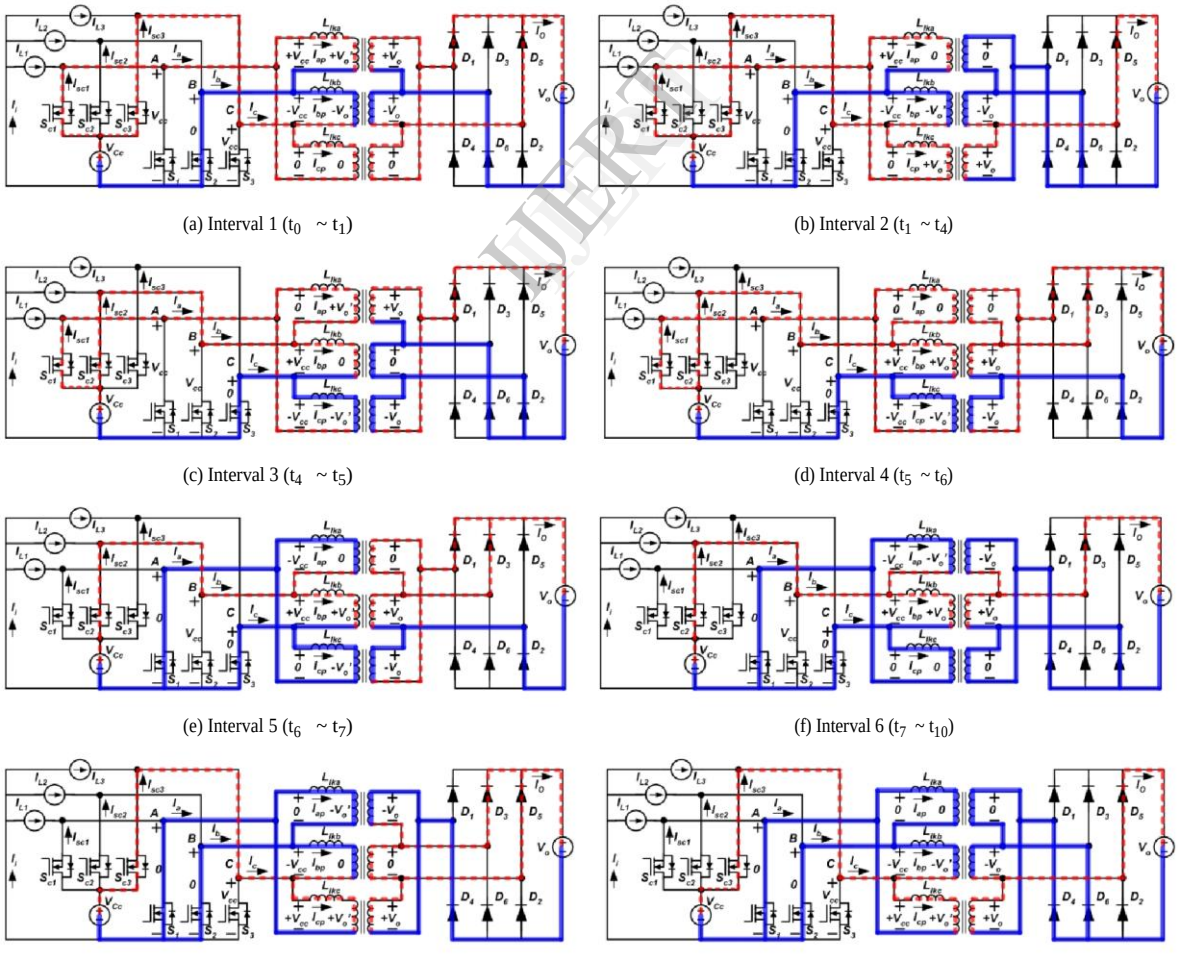

(a) Interval 1 ($t_0 \sim t_1$)
(b) Interval 2 ($t_1 \sim t_4$)
(c) Interval 3 ($t_4 \sim t_5$)
(d) Interval 4 ($t_5 \sim t_6$)
(e) Interval 5 ($t_6 \sim t_7$)
(f) Interval 6 ($t_7 \sim t_{10}$)
(g) Interval 7 ($t_{10} \sim t_{11}$)
(h) Interval 8 ($t_{11} \sim t_0'$)

Figure 4. Eight topological states in phase *A*

$$t_1 - t_0 = \frac{V_{Cc} - V_o'}{V_{Cc}} \frac{T_s}{3} = T_1 \quad (4)$$

$$i_{ap}(t_1) = \frac{V_{Cc}}{L_{lk}} T_1 - i_{ap}(t_0) \quad (5)$$

where $n = N_2/N_1$ (turn-ratio of the transformer), T_S (period), D (duty ratio), $L_{lk} = L_{lka} = L_{lkb} = L_{lkc}$.

$t_1 \sim t_4$ (Fig. 4 (b)) : When the current i_{ap} exceeds i_{cp} at t_1, D_4 turns off and D_1 turns on respectively. Thus, the transformer secondary voltage v_{abs} is changed from zero to $+V_O$ and the current i_{ap} through the leakage inductance L_{lka} increases. The slope is determined by the voltage difference between the clamp voltage $+V_{Cc}$ and the reflected output voltage $+V_O$. Equation (7) shows the interval of current period. Equation (8) evaluates the current i_{ap} at t_4.

$$i_{ap} = \frac{V_{Cc} - V_o'}{L_{lk}} t + i_{ap}(t_1) \quad (6)$$

$$t_4 - t_1 = t_{10} - t_7 = \frac{T_s}{3} - T_1 . \quad (7)$$

$$i_{ap}(t_4) = \frac{V_{Cc} - V_o' - \frac{T_s}{3}}{L_{lk}} T_1 + i_{ap}(t_1) \quad (8)$$

$t_4 \sim t_5$ (Fig. 4 (c)) : At t_4, the phase B main switch S_2 turns off. The primary line-to-line voltage v_{ab} becomes zero and v_{bc} reaches the clamp capacitor voltage $+V_{Cc}$. Thus, the transformer primary current i_{ap} decreases and i_{bp} increases. The transformer primary current i_{ap} through the leakage inductance L_{lka} decreases as a slope determined by $-V_O$ as shown in (9). The interval of this period and the value of $i_{ap}(t_5)$ are same as (4) and (5) respectively.

$$i_{ap} = \frac{V_o'}{L_{lk}} t + i_{ap}(t_4) \quad (9)$$

$t_5 \sim t_6$ (Fig. 4 (d)) : When the current i_{bp} exceeds i_{ap} at t_5, D_6 turns off and D_3 turns on respectively. Thus, the transformer secondary voltage v_{abs} is changed to zero. Since the primary line-to-line voltage v_{ab} keeps remaining to zero, the transformer primary current i_{ap} freewheels through D_1 and D_3. The interval of this period is as shown in (10).

$$t_6 - t_5 = \frac{2}{3} D T_S - T_1 \quad (10)$$

$t_6 \sim t_7$ (Fig. 4 (e)) : At t_6, the phase A main switch S_1 turns on. The primary line-to-line voltage v_{ab} reaches the negative value of V_{Cc} and v_{ca} becomes zero. Thus, the transformer primary current i_{ap} decreases until it reaches the level of $i_{ap}(t_0)$. The current i_{ap} through the leakage inductance L_{lka} decreases as a slope determined by the clamp voltage $-V_{Cc}$ as shown in (11). The interval of this period is equal to T_1 which is the commutation time.

$$i_{ap} = -\frac{V_{Cc}}{L_{lk}} t + i_{ap}(t_1) \quad (11)$$

$$t_7 - t_6 = T_1 \quad (12)$$

$t_7 \sim t_{10}$ (Fig. 4 (f)) : When the current i_{ap} falls below the i_{cp} at t_7, D_1 turns off and D_4 turns on respectively. Thus, the transformer secondary voltage v_{abs} is changed to $-V_O$. The current i_{ap} through the leakage inductance L_{lka} decreases as a slope determined by voltage difference between the negative clamp voltage $-V_{Cc}$ and the reflected negative output voltage $-V_O$ as shown in (13). The interval of this period is same as (7).

$$i_{ap} = -\frac{V_{Cc} - V_o'}{L_{lk}} t + i_{ap}(t_0) \quad (13)$$

$$i_{ap}(t_{10}) = -\frac{V_{Cc} - V_o' - \frac{T_s}{3}}{L_{lk}} T_1 - i_{ap}(t_0) \quad (14)$$

$t_{10} \sim t_{11}$ (Fig. 4 (g)) : At t_{10}, the phase B main switch S_2 turns on. The primary line-to-line voltage v_{ab} becomes zero and v_{bc} reaches the negative value of clamp capacitor voltage, $-V_{Cc}$. Thus, the transformer primary current i_{ap} increases and i_{bp} decreases respectively. The transformer primary current i_{ap} through the leakage inductance L_{lka} increases as a slope determined by $+V_O$ as shown in (15) and i_{bp} through the leakage inductance L_{lkb} decreases as a slope determined by $-V_{Cc}$ as shown in (16). The interval of this period and $i_{ap}(t_{11})$ are same as (4) and $i_{ap}(t_0)$ respectively.

$$i_{ap} = \frac{V_o'}{L_{lk}} t + i_{ap}(t_{10}) \quad (15)$$

$$i_{bp} = -\frac{V_{Cc}}{L_{lk}} t + i_{bp}(t_{10}) \quad -\frac{V_{Cc}}{L_{lk}} t + i_{ap}(t_1) \quad (16)$$

$t_{11} \sim t_0'$ (Fig. 4 (h)) : The modes from interval 1 to 8 in Fig. 4 is repeated periodically and continuously.

The voltage transfer ratio (*VTR*) equation of the proposed converter can be derived by integrating the i_{Sc1} curve with respect to time from t_0 to t_0' as follows.

$$\frac{V_o}{V_i} = \frac{n}{(1 - D)} \frac{B + \sqrt{B^2 + 4}}{2} \quad (17)$$

$$where,\ B = \frac{75 L_{lk}}{R_L T_S}$$

Normalized voltage transfer ratio (*NVTR*) is defined such as (18). It removes an effect of transformer turns-ratio in the overall gain and represents a gain by converter topology.

$$\tilde{V} \quad \frac{V_O}{nV_i} \qquad (18)$$

IV. Simulation and Experimental Results

A. Simulation

Fig. 5 shows simulation waveforms for output power P_O = 500 W, V_i = 30 V and V_O = 370 V, and the waveforms are obtained for a 25 kHz switching frequency (T_S = 40 □sec), 330 □H boost inductor $L_1 \sim L_3$, 13 □H leakage inductance L_{lk}'s and a three-phase transformer which has a 2 mH magnetizing inductance L_m and 1 : 5 turn-ratio (n = 5). Fig. 5 (a) shows the transformer primary current i_{ap} and the currents i_{bp} , i_{cp} in phases *B*, *C* are identical except for a 120^{o} phase displacement. It should be noted that the transformer primary currents flow continuously. Fig. 5 (b) shows the clamp current i_{Sc1}.

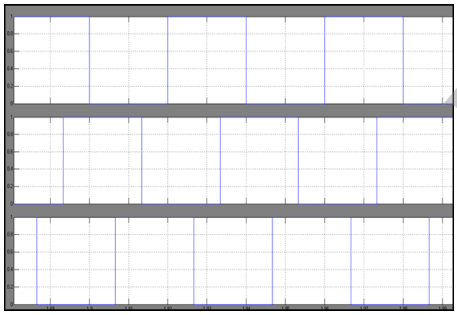

FIGURE 6:PULSES GENERATION

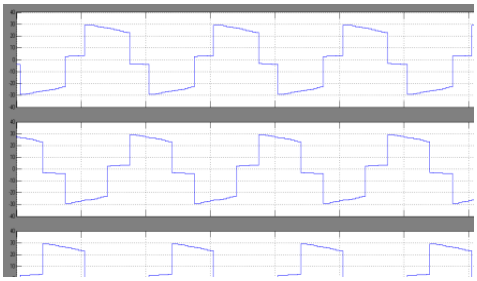

FIG7 : INPUT VOLTAGE

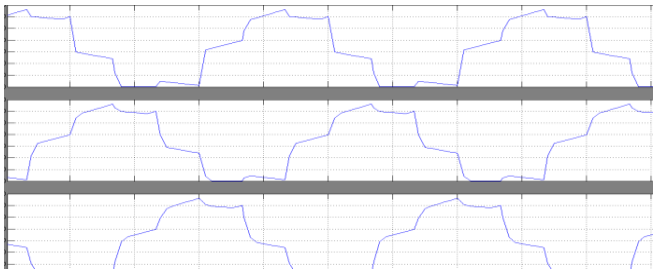

FIG 8: INPUT CURRENT

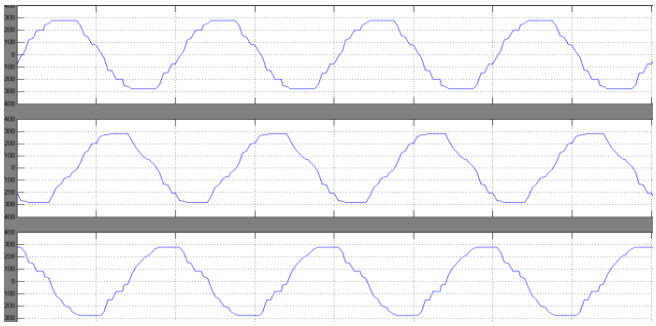

IG9: VOLTAGE IN SECONDARY WINDING OF TRANSFORMER

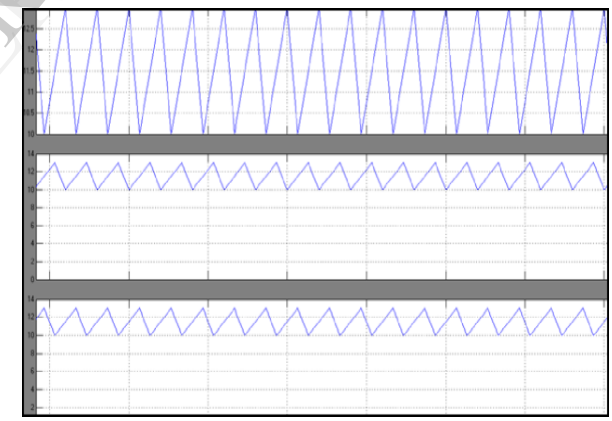

FIG 10 : CURRENT ACROSS THE INDUCTOR

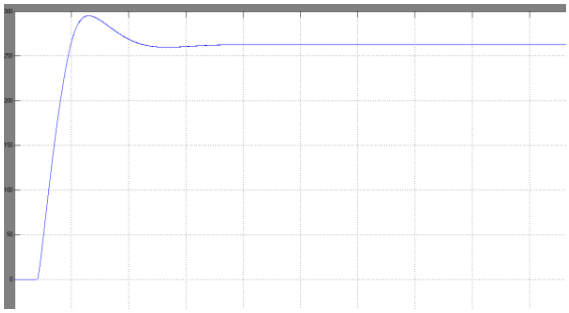

FIG 11:O/P VOLTAGE

B. *Experimental Results*

To verify the proposed converter and PWM strategy, a 500 W prototype unit has been built and tested. It consists of a digital signal processor (DSP: TMS320LF2407) and a field-programmable gate array (FPGA: EPM7128) board to generate PWM patterns for the isolated boost converter; a gate driver board; three legs of main switch branch with active clamp each other; a delta-delta wound three-phase transformer; and three-phase full-bridge rectifiers.

The proposed converter prototype is experimented under 30 V of input voltage and 370 V of output voltage, 500 W load conditions and the same parameters in the simulation are used. Fig. 6 shows the waveforms of transformer primary currents i_{ap}, i_{bp} and i_{cp} at duty $D = 0.6$, where three-phase current waveforms have 120^{o} phase displacement each other and flow in the continuous conduction mode. Fig. 7 shows transformer primary current waveforms in phase *A*, i_{ap} and clamp current i_{Sc1} waveforms, and The waveforms are well matched to the simulation result in Fig. 5. The waveforms in Fig. 8 show interleaved input current i_i and three-phase input boost inductor currents i_{L1}, ~ i_{L3} flowing through boost inductor, L_1 ~ L_3, respectively. The interleaved input current i_i shows typical interleaved operation results; three-times increased switching frequency and reduced ripple magnitude. Fig. 9 shows normalized voltage transfer ratio (*NVTR*) of the proposed converter, where solid line represents calculated data by (17) and "x" marks represent experimented data. The curve in Fig. 10 shows the measured efficiency under loads ranging from 100W to 500W. The efficiency above 96 % is achieved and it is caused by continuous current conduction through transformer and interleaved operation in the three-phase boost converter. Switching losses are reduced by the action of active clamp branches, as well.

V. CONCULSION

A new three-phase dc/dc converter and three-phase PWM strategy have been proposed in this paper. In the proposed converter, interleaved operation of three-phase boost converter reduces overall ripple current, which is imposed into solar cells and thus. The interleaved operation increases effective operating frequency and thus, leads to realization of smaller sized filter components. In addition, the proposed three-phase PWM strategy transfers energy in the continuous conduction mode and three-phase paths. Further, three-phase clamp branch mitigates not only switching losses by zero voltage switching but also electromagnetic noises caused by hard-switched voltage spikes. These characteristics of the proposed converter reduce operating losses significantly and result in the whole converter efficiency above 96%. Inherent voltage boost characteristics of the boost converter increase the voltage transfer ratio in addition to the transformer turns ratio. These advantages make this converter suitable for low dc voltage renewable energy sources such as ultra capacitors.

REFERENCES

[1] M.W. Ellis, M.R. Spakovsky, and D.J. Nelson, "solar cell systems: efficient, flexible energy conversion for the 21st century," *Proceedings of the IEEE*, vol. 89, pp. 1808 – 1818, Dec. 2001

[2] A.R. Prasad, P.D. Ziogas, and S. Manias, "Analysis and design of a three-phase off line DC-DC converter with high-frequency isolation," *IEEE Transactions on Industry Applications*, vol. 28, pp. 824 - 832, July-Aug. 1992

[3] D. de Souza Oliveira and I. Barbi, "A three-phase ZVS PWM DC/DC converter with asymmetrical duty cycle for high power applications," *IEEE Transactions on Power Electronics*, vol. 20, Issue 2, pp. 370 - 377, March 2005

[4] J. Jacobs, A. Averberg, and R. De Doncker, "A novel three-phase dc/dc converter for high-power application," in *Power Electronics Specialists Conference*, 2004, pp. 1861 – 1867

[5] C. Liu, A. Johnson, and J. Lai, "A novel three-phase high-power soft-switched DC/DC converter for low-voltage solar cell applications," *IEEE Transactions on Industry Applications*, vol. 41, pp. 1691 - 1697, Nov.-Dec. 2005

[6] H. Cha, and P. Enjeti, "A novel three-phase high power current-fed dc/dc converter with active clamp for solar cells," in *Power Electronics Specialists Conference*, 2007, pp. 2485 - 2489